A split Hopkinson pressure bar device to carry out confined friction tests under high pressures

Bastien Durand, Franck Delvare, Patrice Bailly, Didier Picart

A SPLIT HOPKINSON PRESSURE BAR DEVICE TO CARRY OUT CONFINED FRICTION TESTS UNDER HIGH PRESSURES

Bastien Durand[1], Franck Delvare[2], Patrice Bailly[3] and Didier Picart[4]

[1]LMT, ENS-Cachan, 94235 CACHAN Cedex, France, bastien.durand@lmt.ens-cachan.fr, +33147402193

[2]Université de Caen, Normandie, Laboratoire N. Oresme, F-14032 Caen, France

[3]INSA CVL, Laboratoire PRISME, F-18020 Bourges, France

[4]CEA, DAM, Le Ripault, F-37260 Monts, France

Abstract: Numerical simulations of mechanical loadings on pyrotechnic structures require the determination of the friction coefficient between steel and explosives. Our study focuses on contact pressures of around 100 MPa and sliding velocities of around 10 m/s. Explosives are brittle materials which fracture when submitted to such pressures in uniaxial compression. They have therefore to be confined to avoid any fracture during the tests. A new Hopkinson bar device which simultaneously enables to confine a sample and rub it on steel has therefore been designed. This device is composed of two coaxial transmission bars. It consists in a cylindrical sample confined in a steel tube, the cylindrical sample being inserted between the incident bar and the internal transmission bar, and the confinement tube being leant against the external transmission bar. The high impedance of the external transmission bar keeps the confinement tube quasi-motionless whereas the impedance of the internal transmission bar is calculated to reach the desired pressure and the desired velocity at the tube-sample interface. Tests have been carried out with an inert material mechanically representative of explosives. The friction coefficient and the stresses at the tube-sample

interface are deduced from strain measurements on the Hopkinson bars and on the external face of the confinement tube, and from an analytical model.

Keywords: friction parameter, identification, confinement, split Hopkinson pressure bars

1 Introduction

Numerical simulations are performed to predict the ignition of confined explosives submitted to accidental impacts [1], [2], [3]. Such impacts are characterised by velocities of several tens of meters per second and are usually called “low-velocity impacts”. These simulations are based on:

- An elasto-plastic model simulating the macroscopic behaviour, whose parameters are identified from triaxial tests.
- A thermo-chemical model enabling the calculation of the local heat due to the irreversible macroscopic strain and due to chemical reactions.

The parameters of the thermo-chemical model are identified from normalised experimental tests supposed to reproduce accidental situations: the drop-weight test [4], the Steven-test [3], [5], [6], the Susan-test [3] and the Taylor test **[7]** among others. Unfortunately, numerical simulations of these normalised tests show that the ignition time of the explosive strongly depends on the friction coefficient at the interface between the explosive and the contact materials (generally steel). A test enabling the friction coefficient measurement between steel and explosives under the “low-velocity impacts” conditions has therefore to be designed.

Numerical simulations display that the “low-velocity impacts” lead to contact pressures reaching 100 MPa and sliding velocities reaching 10 m/s at the interfaces. Few

tribometers satisfy these requirements: tribometer with explosively-driven friction [8], target-projectile assembly with oblique impact [9], Hopkinson torsion bars [10], dynamometrical ring with parallelepipedic specimen launched by a gas gun or an hydraulic machine [11] and the friction of a pin on a revolving disc [12], [13]. With these classical tribometers, mainly used on metals and ceramics, the friction samples are tested in simple compression and this configuration is unfortunately not adapted to our situation, as explained above.

For safety reasons, our friction tests are carried out with an inert material mechanically representative of an explosive. This material is named the I1. The I1 Young's modulus is 2 GPa, its Poisson's ratio ν is estimated to 0.4 and its density is 1850 kg/m^3 [14]. Its inelastic behavior has been studied by carrying out triaxial compression tests [14]. The material flow when its plasticity threshold has been attained (for the sake of simplicity the maximal stresses obtained using triaxial tests are used to define a plasticity threshold). The plasticity flow threshold is defined by a Drucker-Prager criterion [14]:

(1) $\sigma_{mis} - \alpha P < C$

where P is the hydrostatic pressure and σ_{mis} the Von Mises equivalent stress.

Conventionally, the stress in the I1 is positive in compression and negative in traction. A plastic incompressibility and a perfectly plastic behavior (i.e. C constant) are assumed. The parameters have been determined: C = 25 MPa and α = 0.64 [14].

According to relation (1), in the case of a simple compression loading, the maximum axial stress is only 31 MPa. The I1 behavior is quasi-brittle, so when this limit stress is reached, it breaks. The desired 100 MPa pressure cannot therefore be reached with classical

tribometers because of the I1 fracture. The material has therefore to be confined during our tests for two following reasons:

- The behavior of the confined material remains elastic even under high stresses.
- A confinement situation avoids any fracture to occur when the elasticity limit is reached.

A cylindrical I1 sample is thus enclosed in a steel tube. This technique is usually employed to perform compression tests with quasi-uniaxial strain states [14], [15]. Our test bench has to be designed to enables friction to occur between the I1 sample and the steel tube. Our experimental configuration is similar to the compaction tests one [16], [17], [18].

The Hopkinson bar set-up, its potential performances and the friction identification from a test and from an analytical model are described in section 2. Then, the consistency of this identification is verified in section 3 by performing numerical finite element simulations.

2 The Hopkinson bar set-up

2.1 Design and modeling

The Hopkinson bar device used for our friction tests has two coaxial output bars (Figure 1). It consists in an I1 cylindrical sample confined in a steel tube, the sample being inserted between the incident bar (via a plug, see Figure 2) and the internal output bar, and the confinement tube being leant against the external output bar. The high impedance of the external output bar keeps the confinement tube quasi-motionless whereas the impedance of the internal output bar is calculated to reach the desired pressure and the desired velocity at the tube-sample interface. Thus, the steel tube acts both as a confinement, which avoids any

fracture in the I1 sample, and as a friction surface. The radial pressure at the confinement tube – sample interface is generated by the axial compression of the sample.

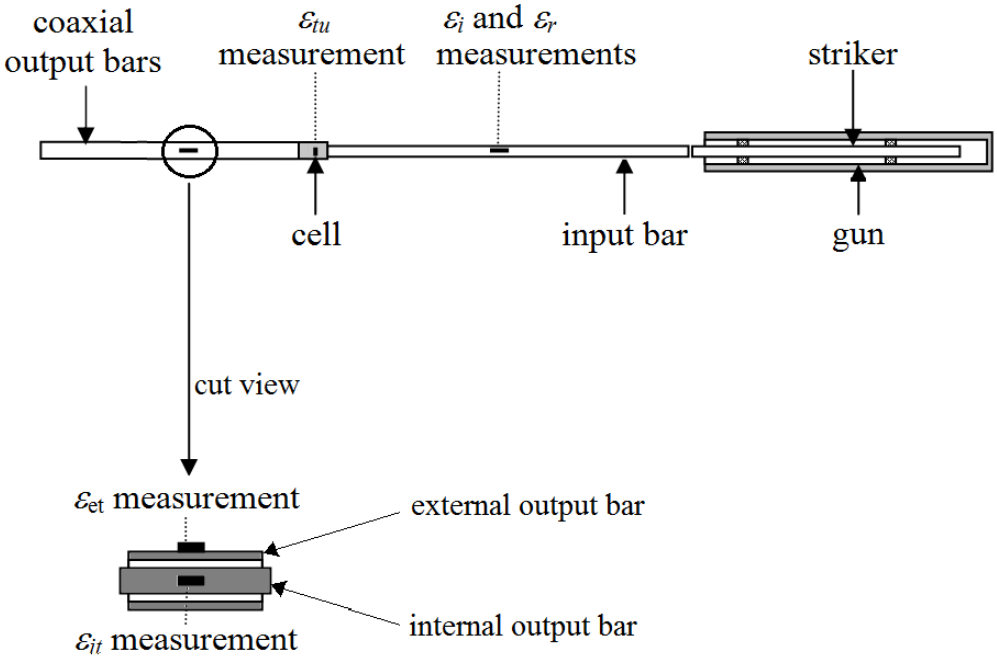

Figure 1: The Split Hopkinson Pressure Bar device. ε_i: incident strain wave, ε_r: reflected strain wave, ε_{tu}: strain measured on the confinement tube, ε_{et}: external transmitted strain wave, ε_{it}: internal transmitted strain wave.

bar	material	Young's modulus	waves celerity	diameters		length
				external	internal	
striker	steel	E_i = 166 GPa	C_i = 4555 m/s	$2R_i$ = 20 mm		1.05 m
input						2.5 m
internal output	aluminum	E_{io} = 72.8 GPa	C_{io} = 5092 m/s	$2R_{io}$ = 10 mm		1.46 m
external output	steel	E_{eo} = 205 GPa	C_{eo} = 5162 m/s	$2R_{eeo}$ = 40 mm	$2R_{ieo}$ = 30 mm	1.5 m

Table 1: Young's moduli, tensile/compressive waves celerities, diameters and lengths of the bars.

The impact of the striker induces an incident compressive strain wave ε_i in the input bar (Figure 1). Reverberation occurs in the cell (cell details are given on Figure 2), which leads to a reflected strain wave ε_r in the input bar, to a transmitted compressive strain wave ε_{it} in the internal output bar and to a transmitted compressive strain wave ε_{et} in the external output bar. ε_i and ε_r are both measured by a longitudinal strain gauge glued on the input bar, at 1.22 m from the plug interface, where the two waves are separated in time. ε_{it} is measured by a longitudinal strain gauge glued at 330 mm from the sample interface and ε_{et} is measured by a longitudinal strain gauge glued on the external face of the external output bar and at 295 mm from the confinement tube interface.

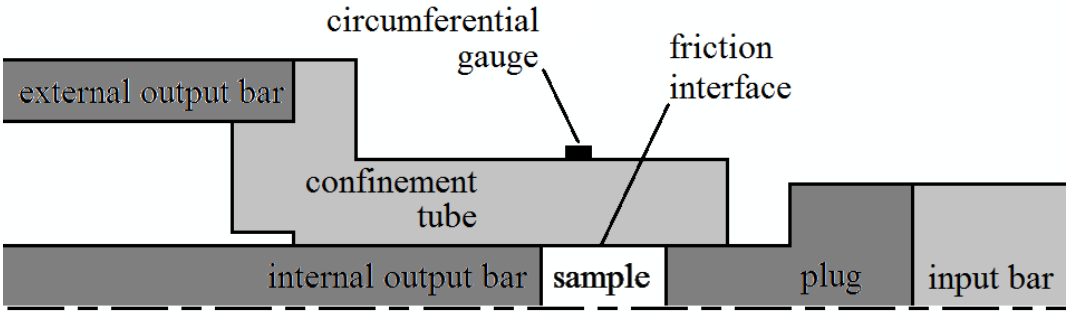

Figure 2 : Zoom on the mounting with the cell composed of the plug, the sample and the confinement tube (axisymmetric cut view).

The sample has a diameter $2R$ and a length L equal to 10 mm, the confinement tube has an external diameter $2R_t$ equal to 24 mm and the length scale is respected on Figure 2. The confinement tube and the plug, made of steel, have a Young's modulus E_t and a Poisson's ratio ν_t respectively equal to 200 GPa and to 0.29. The friction face of the confinement tube has been reamed and the sample was turned on a sliding lathe. Both have a weak surface roughness representative of the pyrotechnic structures roughness (arithmetic average of absolute values R_a roughly equal to 0.8). The radial clearance between the plug and the tube and between the internal output bar and the tube is of the order of 0.01 mm. Teflon sheets have been inserted between the plug and the sample and between the internal output bar and the sample in order to reduce the friction at these interfaces and thus increase the pressure at the tube-sample interface. The circumferential gauge glued on the confinement tube is 2 mm wide. The initial axial distance between the sample middle and the gauge middle is chosen equal to 2.5 mm because the sample displacement relatively to the tube during the test is supposed to be around 5 mm. Thus, the gauge is glued at the mean axial position of the sample middle.

The force F_i applied by the input bar on the plug and the velocity V_i at the input bar - plug interface can be determined from the Hopkinson formulae (2) and from strain waves ε_i and ε_r measured by the gauge and virtually transported at the input bar - plug interface (see Table 1 for symbols definitions):

(2) $$\begin{cases} F_i = -\pi R_i^{\,2} E_i \left(\varepsilon_i + \varepsilon_r\right) \\ V_i = C_i \left(\varepsilon_r - \varepsilon_i\right) \end{cases}$$

The force F_{io} applied by the internal output bar on the sample and the velocity V_{io} at the internal output bar - sample interface can be determined from the Hopkinson formulae (3) and from strain wave ε_{it} measured by the gauge and virtually transported at the internal output bar - sample interface:

(3) $$\begin{cases} F_{io} = -\pi R_{io}^{\,2} E_{io} \varepsilon_{it} \\ V_{io} = -C_{io} \varepsilon_{it} \end{cases}$$

The force F_{eo} applied by the external output bar on the confinement tube and the velocity V_{eo} at the external output bar – confinement tube interface can be determined from the Hopkinson formulae (4) and from strain wave ε_{et} measured by the gauge and virtually transported at the external output bar – confinement tube interface:

(4) $$\begin{cases} F_{eo} = \pi \left(R_{ieo}^2 - R_{eeo}^2\right) E_{eo} \varepsilon_{et} \\ V_{eo} = -C_{eo} \varepsilon_{et} \end{cases}$$

The equilibrium state of the cell (i.e. the confinement tube, the sample and the plug) gives:

(5) $F_i = F_{eo} + F_{io}$

The stationary state of the cell gives:

(6) $V_i = V_{io}$

In the case of a stationary state, the sliding velocity at the friction interface V can be expressed as following:

(7) $V = V_{io} - V_{eo}$ or $V = V_i - V_{eo}$

The sample behavior has to be modeled to obtain a second relation between the forces F_i, F_{eo} and F_{io}. The model used is similar of the Janssen's one [19] and has been previously used by the authors in [20] and [21]. The approach is based on three assumptions:

(i) the confinement tube is assumed to be perfectly rigid,

(ii) the sample behavior remains elastic,

(iii) in the sample, the axial, radial and circumferential stresses and strains do not depend on the radial coordinate.

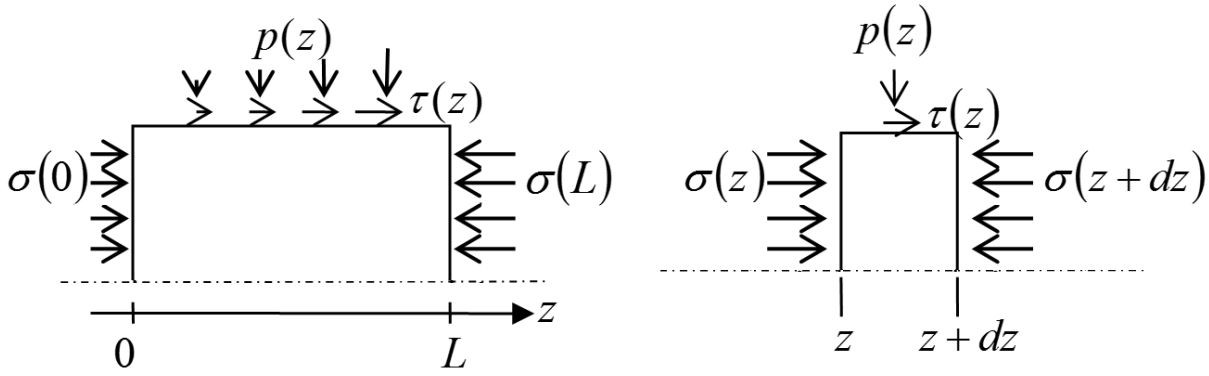

Figure 3: Stresses in the sample. *z*: axial coordinate, *p(z)*: radial pressure, *τ(z)*: friction stress applied by the tube on the interface, *σ(z)*: axial stress.

If the stresses in the sample (Figure 3) are positive in compression and negative in traction, the Hooke's law leads to the following relation:

$$\frac{p(z)}{\sigma(z)} = \frac{\nu}{1-\nu} \quad (8)$$

ν being the I1 Poisson's ratio.

The axial equilibrium of the sample slice between *z* and *z+dz* (Figure 3) leads to:

$$2\tau(z) = R\sigma'(z) = R\frac{d\sigma(z)}{dz} \quad (9)$$

R being the sample radius.

A Coulomb's law with a friction coefficient denoted *f* at the tube-sample interface leads to:

$$\tau(z) = f\ p(z) \quad (10)$$

The relations (8), (9) and (10) lead to a differential equation:

$$\frac{\sigma'(z)}{\sigma(z)} = \frac{2 f \nu}{R(1-\nu)} \quad (11)$$

By taking into account the boundary conditions:

$$\begin{cases} F_i = \pi\ R^2 \sigma(L) \\ F_{io} = \pi\ R^2 \sigma(0) \end{cases} \quad (12)$$

we obtain:

$$\frac{F_i}{F_{io}} = \exp(\beta\ f) \text{ with } \beta = \frac{2\nu\ L}{R(1-\nu)} \quad (13)$$

The incident strain wave ε_i can be linked to the impact velocity of the striker V_s:

$$\varepsilon_i = -\frac{V_s}{2C_i} \quad (14)$$

Thanks to the Hopkinson formulae (2), (3) and (4), thanks to the equilibrium state equation (5), thanks to the stationary state equation (6), and thanks to relation (13), the mean pressure along the friction interface p_{mean} and the sliding velocity V can be determined from the impact velocity of the striker V_s, from the friction coefficient f and from the set-up parameters:

(15) $$p_{mean} = \frac{R_i^{\,2} R_{io}^{\,2} E_i \, E_{io} \left[\exp(\beta \, f) - 1\right]}{2 f \, R \, L \left[R_i^{\,2} E_i \, C_{io} + R_{io}^{\,2} E_{io} \, C_i \exp(\beta \, f)\right]} V_s$$

(16) $$V = \frac{R_i^{\,2} E_i \left\{ C_{io} - \dfrac{R_{io}^{\,2} E_{io} \, C_{eo} \left[\exp(\beta \, f) - 1\right]}{\left(R_{eeo}^2 - R_{ieo}^2\right) E_{eo}} \right\}}{R_i^{\,2} E_i \, C_{io} + R_{io}^{\,2} E_{io} \, C_i \exp(\beta \, f)} V_s$$

Relations (15) and (16) enable to choose the apparatus dimensions (L, R, R_i, R_{io}, R_{eeo} and R_{ieo}), the apparatus materials (E_i, C_i, E_{io}, C_{io}, E_{eo} and C_{eo}) and the striker initial velocity V_s knowing the sample Poisson's ratio ν, the friction coefficient f and the desired interface solicitations (p_{mean} and V). It must be highlighted that an accurate calculation of the apparatus needs to know a priori an order of the friction coefficient f magnitude and needs to know accurately the sample Poisson's ratio ν. The striker of our apparatus can be launched at 10 m/s. Figure 4 therefore displays the magnitudes of the mean pressure and of the sliding velocity that can be reached with our set-up. Figure 4 shows that the mean pressure increases and that the sliding velocity decreases when the friction coefficient increases. The desired 100 MPa pressure and the desired 10 m/s sliding velocity can almost be simultaneously approached for very low friction coefficients (lower than 0.1). It could be noted that the pressure and the sliding velocity cannot be simultaneously imposed to a desired value because one depends on the other.

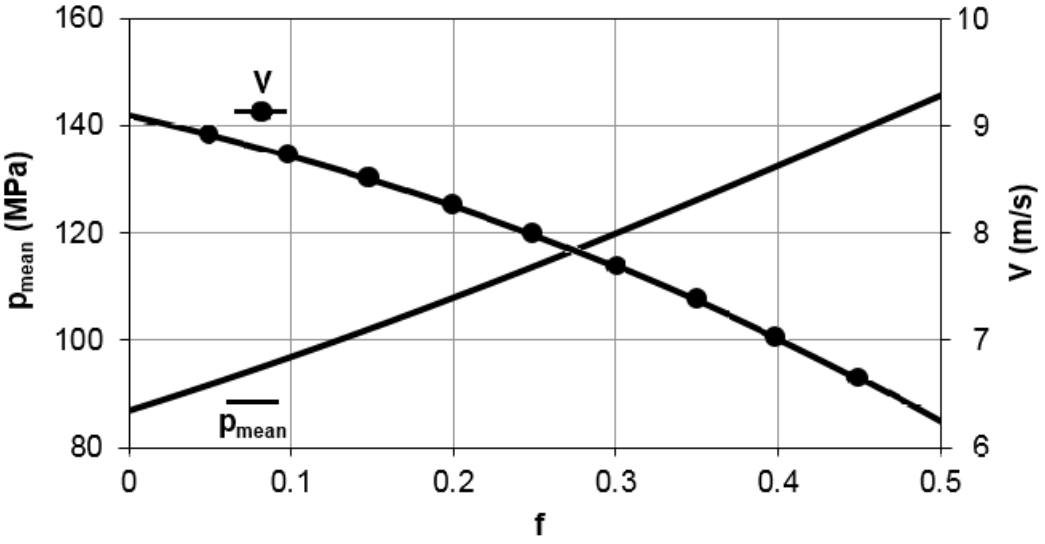

Figure 4 : Evolution of the mean pressure p_{mean} and of the sliding velocity V as a function of the friction coefficient f.

None of the former devices enables to reach such friction solicitations. The tribometer used in [20] enables to reach a sliding velocity of around 10 m/s but limits the mean pressure to 20 MPa whereas the tribometer used in [21] and in [22] enables to reach a mean pressure of around 100 MPa but limits the sliding velocity to 2 m/s.

2.2 Analysis of measurements

A test has been conducted to experimentally check if the sample reaches a stationary equilibrium state as assumed in section 2.1. The time evolutions of the raw strains are shown on Figure 5. The forces applied by the bars on the cell and the velocities at the bars-cell interfaces are then determined from the Hopkinson formulae (2), (3) and (4). The input force can be compared to the output force on Figure 6 and the sample input velocity can be compared to the sample output velocity on Figure 7.

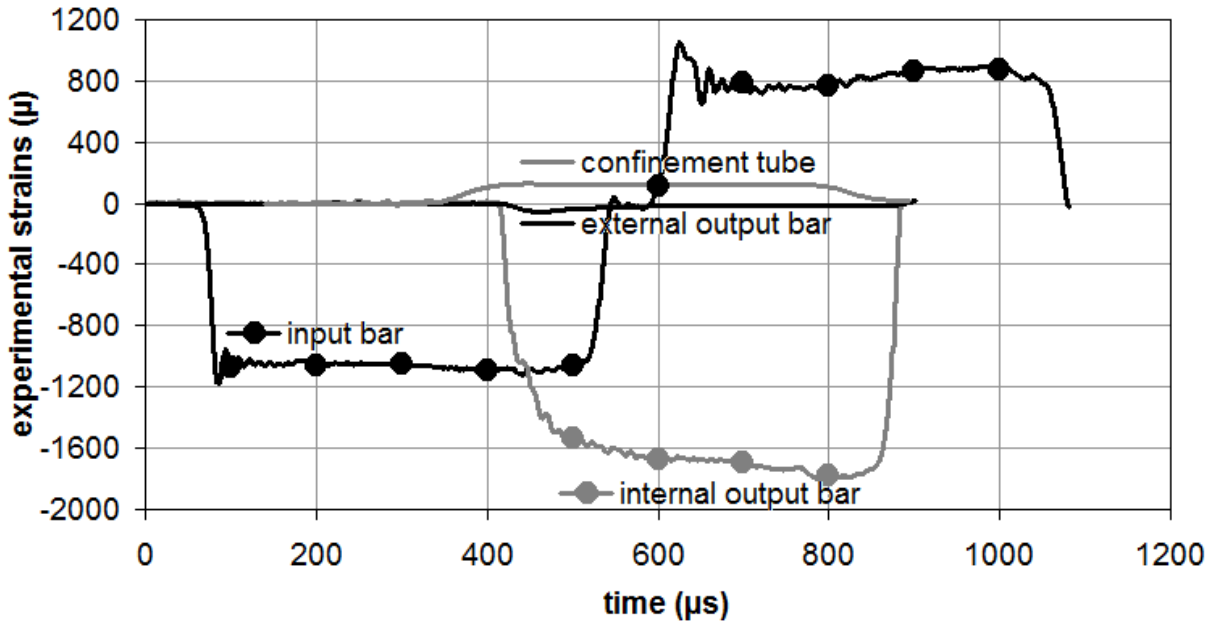

Figure 5: Time evolutions of the raw strains measured by the gauges glued on bars and on the confinement tube. The strain measured on the external output bar is very low compared to the others.

We can notice that the time beginning used on Figure 5 is different from the one used on the other figures and will be no more used in the paper.

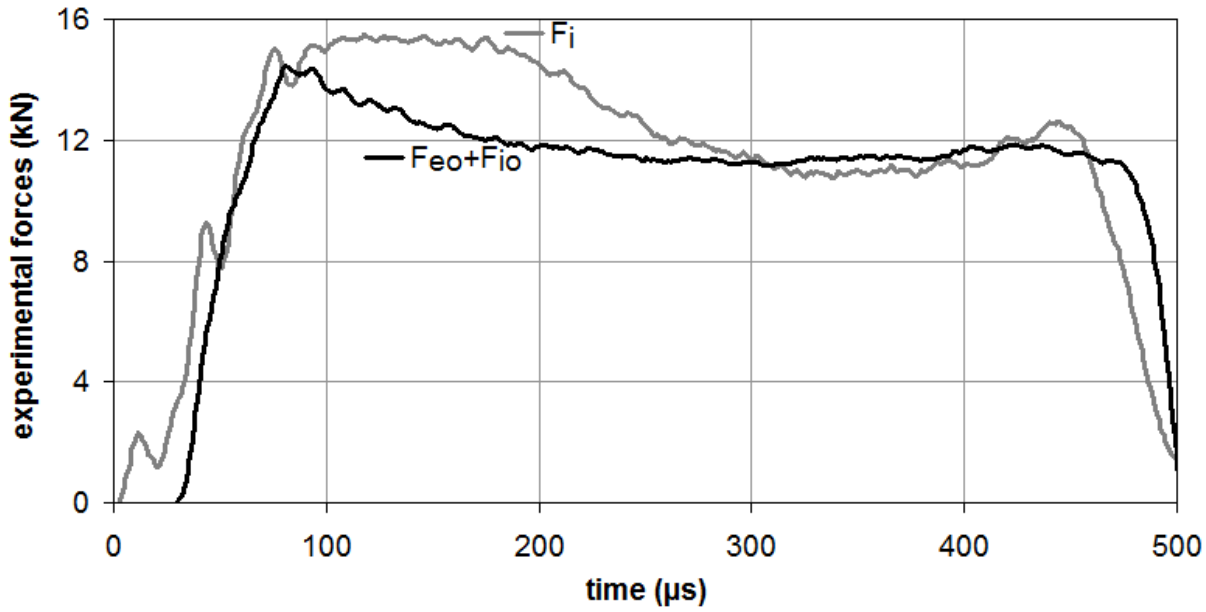

Figure 6: Time evolutions of the input force F_i and of the sum of the external output force and of the internal output force $F_{eo}+F_{io}$ deduced from the measured strain waves in the bars and from the Hopkinson formulae.

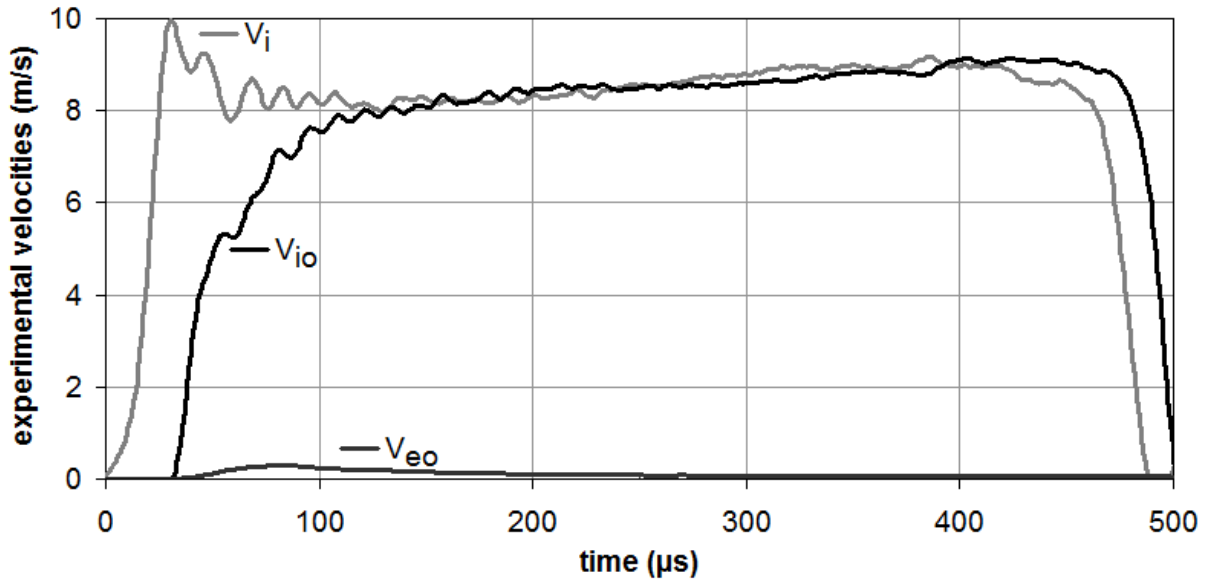

Figure 7: Time evolutions of the input velocity V_i, of the internal output velocity V_{io} and of the external output velocity V_{eo} deduced from the measured strain waves in the bars and from the Hopkinson formulae.

A quite satisfactory stationary equilibrium state can be observed on Figure 6 and Figure 7. The evolution of the experimental input force F_i during the transient phase (at the beginning) can be explained by the time shifting of the incident and the reflected waves ε_i and ε_r. These two waves being quasi-opposed (Figure 8), uncertainties are amplified when the input force is calculated with formula (2). The experimental evolution of F_i will therefore not be used to identify the friction coefficient f and we will focus only on the stationary phase (approximately from 300 µs to 400 µs).

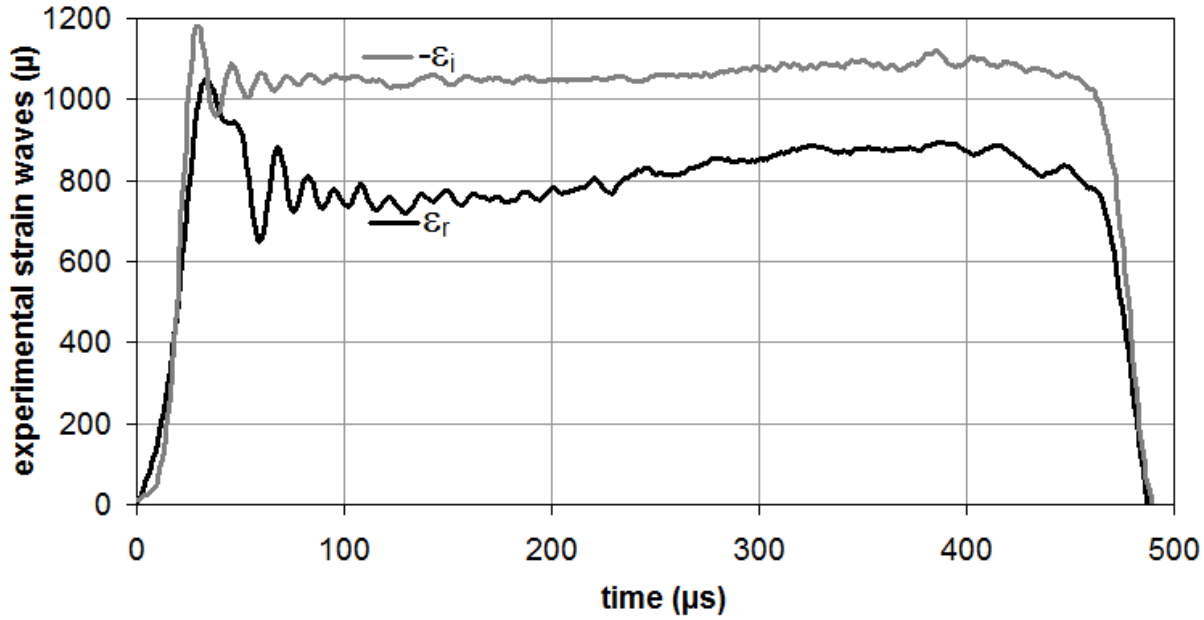

Figure 8: Time evolutions of the opposite of the measured incident strain wave ε_i and of the measured reflected wave ε_r, both virtually transported at the input bar - plug interface.

Figure 7 shows that the sliding velocity V is of the order of 8-9 m/s during the stationary phase.

According to relations (5) and (13), the friction coefficient f can be deduced from the output forces ratio $\frac{F_{eo}}{F_{io}}$:

$$f = \frac{\ln\left(\frac{F_{eo}}{F_{io}} + 1\right)}{\beta} \quad (17)$$

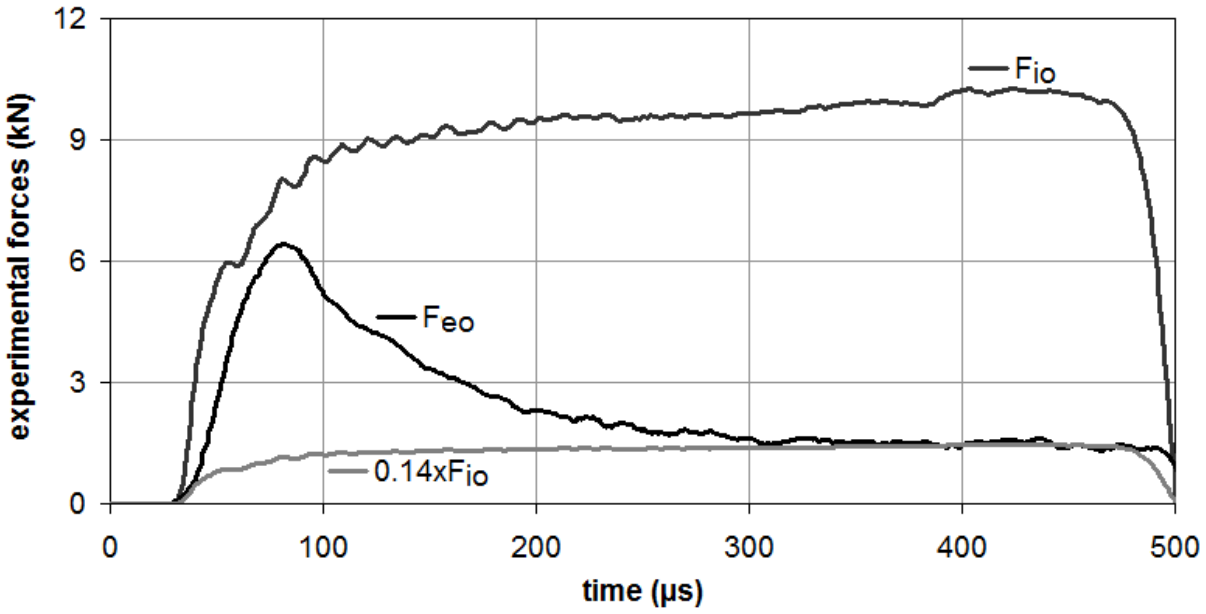

Figure 9: Time evolutions of the external output force F_{eo} and of the internal output force F_{io} deduced from the measured strain waves in the bars and from the Hopkinson formulae.

The $\frac{F_{eo}}{F_{io}}$ ratio identified during the stationary phase on Figure 9 in roughly 0.14. By using relation (17), it leads to $\beta f \approx 0.13$ and if $\nu \approx 0.4$ to $f \approx 0.05$.

The mean friction stress τ_{mean} can be deduced from F_{eo} which corresponds to the friction force:

(18) $$\tau_{mean} = \frac{F_{eo}}{2\pi RL}$$

The minimal pressure p_{min} is reached on $z = 0$ and the maximal pressure p_{max} in reached on $z = L$ (Figure 3). According to relations (5), (8) and (12), p_{min} and p_{max} can be expressed from the output forces F_{eo} and F_{io}:

(19) $$\begin{cases} p_{\min} = p(0) = \dfrac{\nu}{1-\nu}\dfrac{F_{io}}{\pi R^2} \\ p_{\max} = p(L) = \dfrac{\nu}{1-\nu}\dfrac{F_{eo}+F_{io}}{\pi R^2} \end{cases}$$

According to relations (8), (9) and (10), the pressure p is an exponential function of $(f z)$:

(20) $$p = p_{mean}\frac{\beta\ f \exp\left(\dfrac{\beta\ f\ z}{L}\right)}{\exp(\beta\ f)-1}$$

For low magnitudes of f, p can thus be considered as an affine function of z, which implies:

(21) $$p_{mean} = \frac{p_{\min} + p_{\max}}{2}$$

The mean interface stresses are determined from the experimental output forces F_{eo} and F_{io}, from relations (19) and from relation (21):

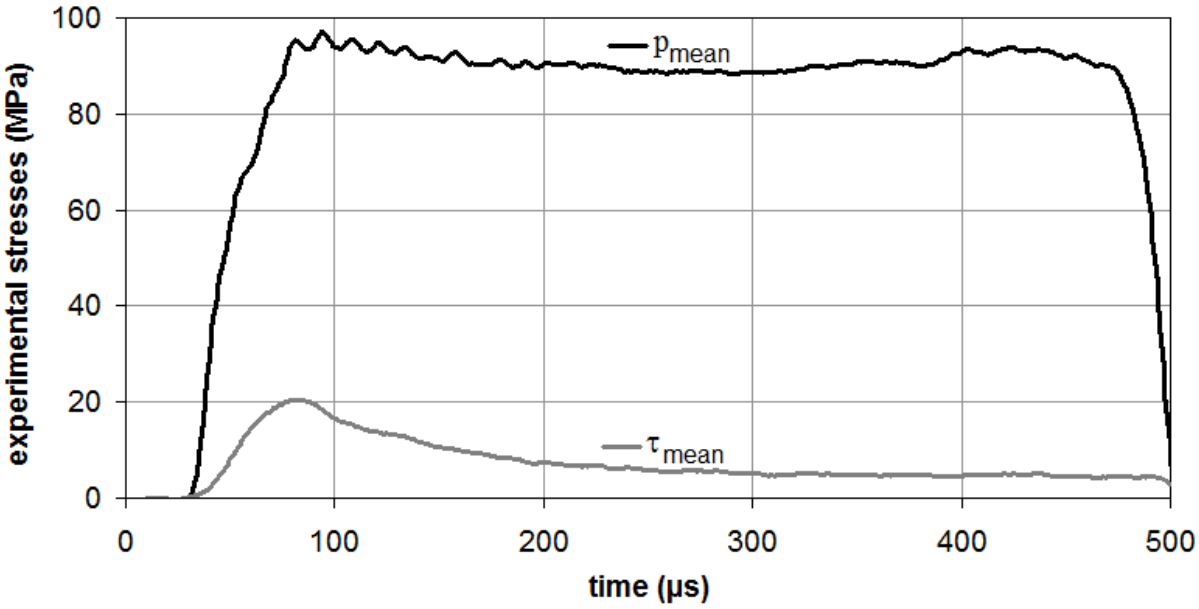

Figure 10: Time evolutions of the experimental mean pressure p_{mean} and of the experimental mean friction stress τ_{mean}.

Figure 10 shows that the mean pressure p_{mean} is of the order of 90-100 MPa.

3 Numerical simulations of the test: check of the results consistency

Finite element simulations (software: ABAQUS/Explicit) are performed in order to check the consistency of the experimental results and of the friction coefficient magnitude identified from our analytical model ($f \approx 0.05$). The whole set-up except for the striker is exactly reproduced in these simulations. As Teflon sheets have been inserted between the plug and the sample and between the internal output bar and the sample, these contacts are supposed to be frictionless. The experimental incident strain wave ε_i is used as an imposed loading by applying on the right-hand extremity of the input bar (Figure 1) a pressure equal to the opposite of the measured strain ε_i virtually transported at the extremity multiplied by the

input bar Young's modulus E_i. The opposite of ε_i can be seen on Figure 8. The strains ε_r, ε_{tu}, ε_{et} and ε_{it} can be considered as the mechanical response of the set-up to ε_i and the simulations have been performed with several values of the friction coefficient f to study its influence on the response.

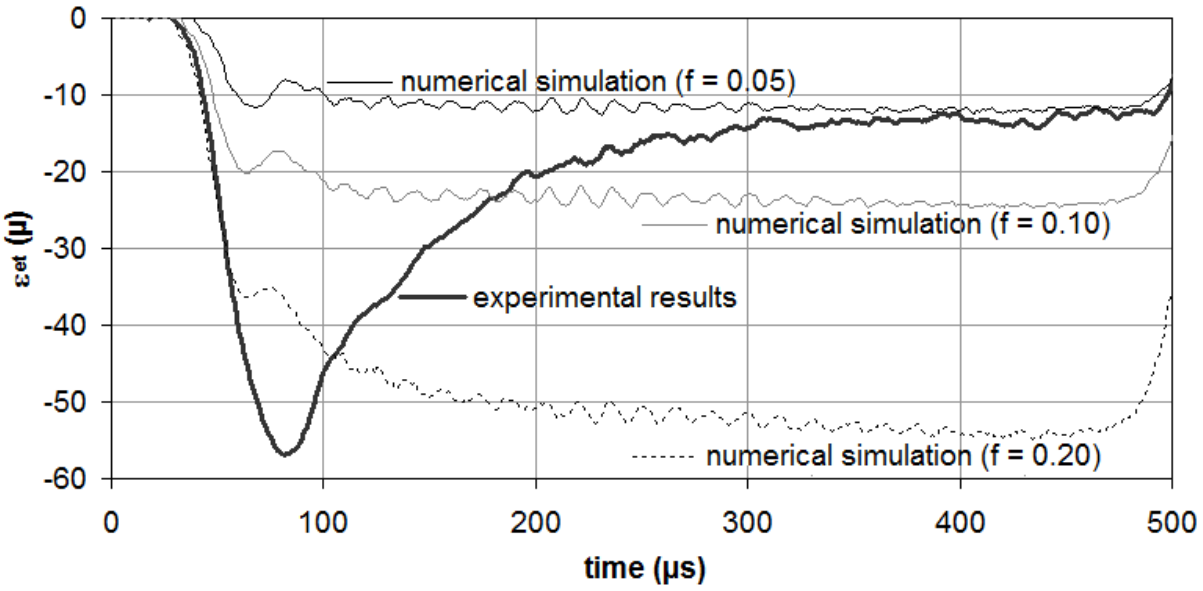

Figure 11: Time evolution of the measured external transmitted strain wave ε_{et} virtually transported at the external output bar – confinement tube interface and its numerical equivalent depending on the friction coefficient f magnitude.

The numerical equivalent of the strain measured by the gauge glued on the confinement tube ε_{tu} is actually the mean value of the numerical circumferential strain along the gauge width.

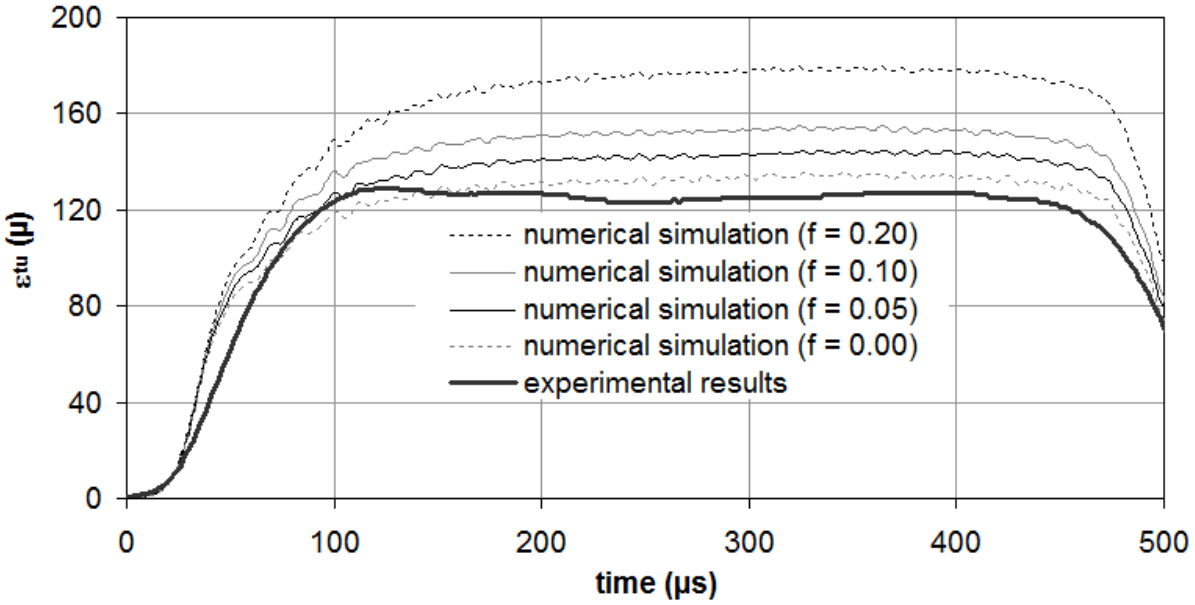

361

362 Figure 12: Time evolution of the strain measured by the gauge glued on the confinement tube

363 ε_{tu} and its numerical equivalent depending on the friction coefficient *f* magnitude.

364

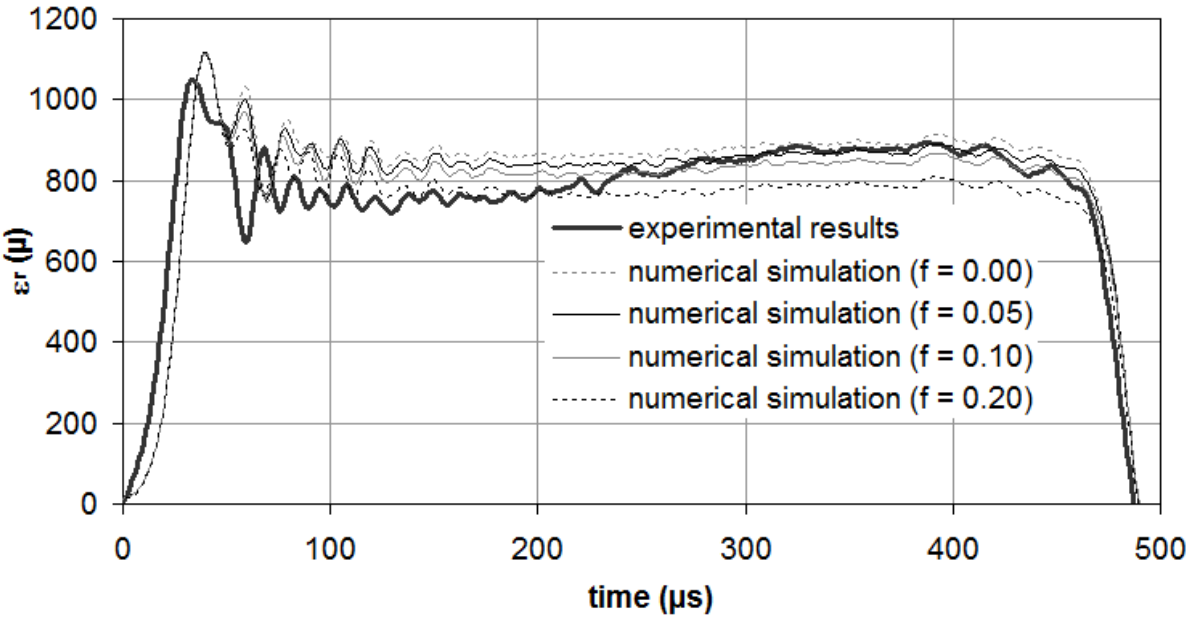

365

366 Figure 13: Time evolution of the measured reflected strain wave ε_r virtually transported at the

367 input bar - plug interface and its numerical equivalent depending on the friction coefficient *f*

368 magnitude.

369

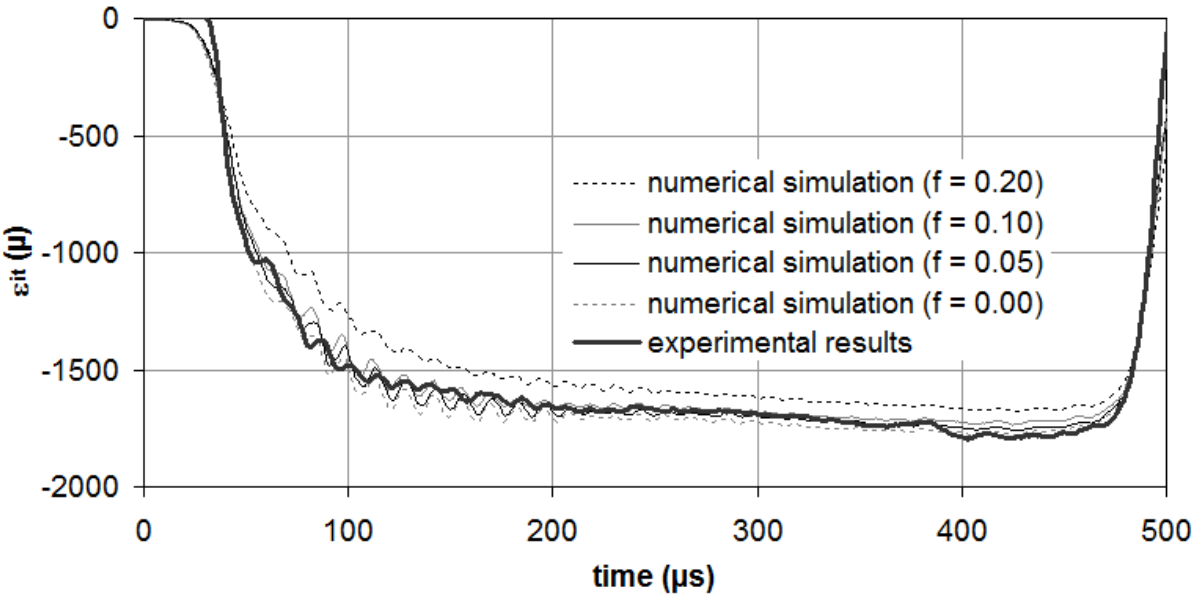

Figure 14: Time evolution of the measured internal transmitted strain wave ε_{it} virtually transported at the internal output bar - sample interface and its numerical equivalent depending on the friction coefficient *f* magnitude.

The external transmitted strain wave ε_{et} is proportional to the friction force and is therefore the most friction dependent strain (Figure 11). During the stationary phase, $f = 0.05$ is a very good fit with the experimental ε_{et}. The strain measured on the confinement tube ε_{tu} is also highly dependent on *f*, but a perfect fit cannot be obtained because of the numerical strains high values (Figure 12). The reflected strain wave ε_r and the internal transmitted strain wave ε_{it} are quasi-independent on friction (Figure 13 and Figure 14). During the stationary phase, $f = 0.05$ is consistent with the measured ε_r and with the measured ε_{it}.

4 Discussion of the analytical model assumptions

Relation (17) leads to the following one:

(22) $[\exp(\beta f)-1]F_{io} = F_{eo}$

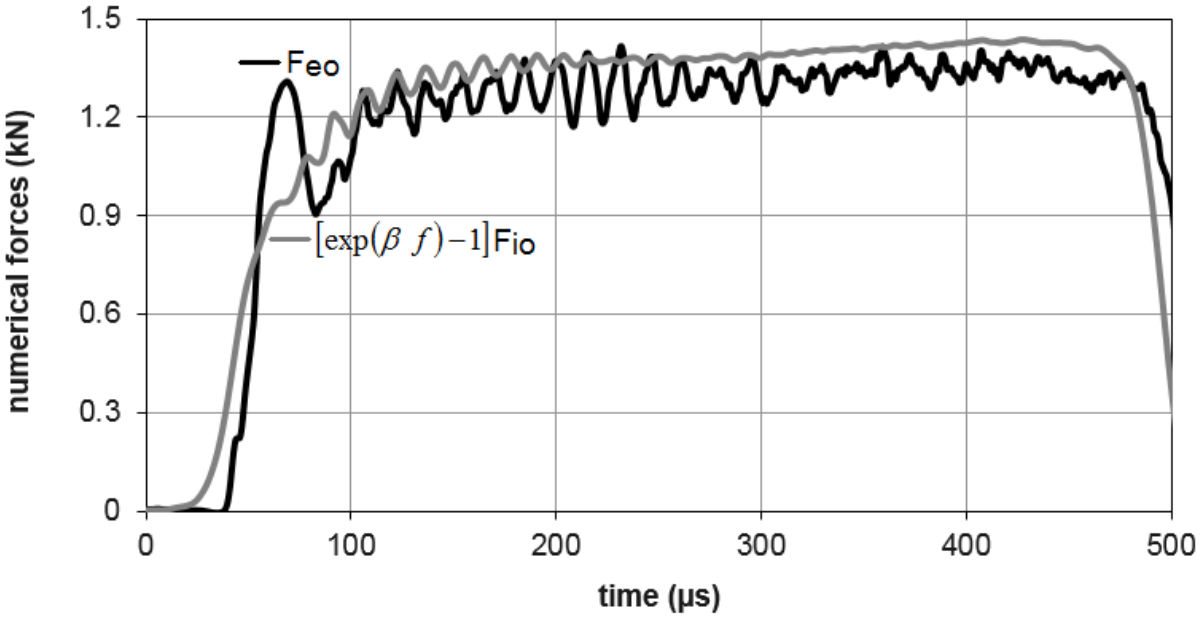

Figure 15: Time evolutions of the numerical external output force F_{eo} and of $[\exp(\beta f)-1]F_{io}$ (with f = 0.05).

Figure 15 shows that the analytical model slightly overestimates the friction force F_{eo}. Only this criterion finally matters because f is firstly identified from the $\frac{F_{eo}}{F_{io}}$ ratio.

5 Conclusion

The purpose was to design a set-up enabling the friction measurement between an inert material, mechanically representative of explosives, and a steel confinement. The desired sliding velocities and the desired pressures were respectively 10 m/s and 100 MPa. A confinement set-up using the split Hopkinson pressure bars technique had to be designed because of the low mechanical resistance of the inert material when submitted to the simple

compression of classical tribometers. Such a configuration does not enable to make direct measurements. As a result, the stresses and the friction coefficient at the interface between steel and the inert material were identified from indirect measurements, from an analytical model and from the value of the inert material Poisson's ratio. It has been shown that the sliding velocity and the pressure reached roughly 8-9 m/s and 90-100 MPa whereas the striker was launched at only 10 m/s.

A very low friction coefficient has been measured: only 0.05. In [20] and [21], a sliding velocity of the order of 1 mm/min has been imposed and the corresponding friction coefficient is roughly 0.2. In [22], the mean pressure is approximately 70 MPa and the sliding velocity is of the order of 2 m/s. In [20], the mean pressure is approximately 20 MPa and the sliding velocity is around 10 m/s. In both cases, the friction coefficient is of the order of 0.4-0.5. The reasons of such a variation should be studied in a future work. The friction drop at the very beginning of the test could also be studied by using a time dependent friction model.

The measurements processing could also be improved by using an inverse method like in [23]. Another prospect is the design of a compaction test enabling the friction force measurement. Indeed, the study of the friction in compaction situations is an issue [16], [18] and our device enables the simultaneous determination of the friction parameters and of the compacted material parameters.

Acknowledgments: The authors would like to thank Maxime Biessy for his help and the reviewers for their valuable comments.

6 References

[1]: Picart D, Delmaire-Sizes F, Gruau C, Trumel H. Ignition of a HMX-based PBX submitted to impact: strain localisation and boundary condition. 16th Conference of the American Physical Society Topical Group on Shock Compression of Condensed Matter (2009).

[2]: Picart D, Bouton E. Non-shock ignition of a HMX-based high explosive: thermo-mechanical numerical study. 14th International Detonation Symposium, Coeur d'Alène, USA (2010).

[3]: Picart D, Ermisse J, Biessy M, Bouton E, Trumel H. Modelling and simulation of plastic-bonded explosive mechanical initiation. International Journal of Energetic Materials and Chemical Propulsion, 12(6), 487-509 (2013).

[4]: Field JE, Swallowe GM, Heaven SN. Ignition mechanisms of explosives during mechanical deformations. Proceeding of the Royal Society London A, 383, 231-44 (1982).

[5]: Gruau C, Picart D, Belmas R, Bouton E, Delmaire-Sizes F, Sabatier J, Trumel H. Ignition of a confined high explosive under low velocity impact. International Journal of Impact Engineering 36, 537–550 (2008).

[6]: Vandersall KS, Chidester SK, Forbes JW, Garcia F, Greenwood DW, Switzer LL and al. Experimental and modelling studies of crush, puncture, and perforation scenarios in the Steven impact test. Office Naval Research 333-05-02, (Eds.), Proceedings of the 12th International Detonation Symposium, San Diego, 131–139 (2002).

[7]: Yodo A and al. Energetic materials for defense - Safety, vulnerability - Friability. AFNOR NF EN 16701 (2014).

[8]: Kim HJ, Emge A, Winter RE, Keightley PT, Kim WK, Falk ML, Rigney DA. Nanostructures generated by explosively driven friction: Experiments and molecular dynamics simulations. Acta Materiala, 57(17), 5270-5282 (2009).

[9]: Rajagopalan S, Irfan MA, Prakash V. Novel experimental techniques for investigating time resolved high speed friction. Wear, 225-229, Part 2, 1222-1237 (1999).

[10]: Huang H, Feng R. Dynamic Friction of SiC Surfaces: A Torsional Kolsky Bar Tribometer Study. Tribology Letters, 27, 329-338 (2007).

[11]: Philippon S, Voyiadjis GZ, Faure L, Lodygowski A, Rusinek A, Chevrier P, Dossou E. A Device Enhancement for the Dry Sliding Friction Coefficient Measurement Between Steel 1080 and VascoMax with Respect to Surface Roughness Changes. Experimental Mechanics, 51(3), 337-358 (2011).

[12]: Dickson PM, Parker GR, Smilowitz LB, Zucker JM, Asay BW. Frictional Heating and Ignition of Energetic Materials. CP845, Conference of the American Physical Society Topical Group on Shock Compression of Condensed Matter, 1057-1060 (2005).

[13]: Hoffman DM, Chandler JB. Aspect of the tribology of the plastic bonded explosive LX-04. Propellants, Explosives, Pyrotechnics 29, 368–373 (2004).

[14]: Bailly P, Delvare F, Vial J, Hanus JL, Biessy M, Picart D. Dynamic behavior of an aggregate material at simultaneous high pressure and strain rate: SHPB triaxial tests. International Journal of Impact Engineering, 38, 73-84 (2011).

[15]: Forquin P, Safa K, Gary G. Influence of free water on the quasi-static and dynamic of strength of concrete in confined compression tests. Cement and Concrete Research, 40, 321-333 (2009).

[16]: Azhdar B, Stenberg B, Kari L. Determination of dynamic and sliding friction, and observation of stick-slip phenomenon on compacted polymers during high velocity compaction. Polymer Testing, 25, 1069–1080 (2006).

[17]: Burlion N, Pijaudier-Cabot G, Dahan N. Experimental analysis of compaction of concrete and mortar. International Journal for Numerical and Analytical Methods in Geomechanics, 25(15), 1467-1486 (2001).

[18]: Yong-Ming Tien, Po-Lin Wu, Wei-Hsing Huang, Ming-Feng Kuo, Chen-An Chu. Wall Friction measurement and compaction characteristics of bentonite powders. Powder Technology 173, 140-151 (2007).

[19]: Janssen HA. Versuche über Getreiedruch in Silozellen. Vereins Z Deutsch Eng 39, 1045 (1895).

[20]: Durand B, Delvare F, Bailly P, Picart D. Friction between steel and a confined inert material representative of explosives under severe loadings. Experimental Mechanics DOI 10.1007/s11340-014-9885-z (2014).

[21]: Durand B, Delvare F, Bailly P, Picart D. Identification of the friction under high pressure between an aggregate material and steel: experimental and modelling aspects. International Journal of Solids and Structures, 50(24), 4108-4117 (2013).

[22]: Durand B, Delvare F, Bailly P, Picart D. A friction test between steel and a brittle material at high contact pressures and high sliding velocities. 10th International DYMAT Conference (2012).

[23]: Durand B, Delvare F, Bailly P. Numerical solution of Cauchy problems in linear elasticity in axisymmetric situations. International Journal of Solids and Structures, 21, 3041-3053 (2011).